Room Temperature Slot-Die Coated Perovskite Layer Modified with sulfonyl-γ-AApeptide for High Performance Perovskite Solar Devices

Seid Yimer Abate[a,1], Ziqi Yang[b,1], Surabhi Jha[c], Guorong Ma[c], Zhongliang Ouyang[d], Haixin Zhang[e], Shafi Muhammad[a], Nihar Pradhan[a], Xiaodan Gu[c], Derek Patton[c], Kun Wang[e] Dawen Li[d], Jianfeng Cai[b,] and Qilin Dai[a,*]*

[a] *Department of Chemistry, Physics, and Atmospheric Sciences, Jackson State University, Jackson, MS, 39217, United States*

[b] *Department of Chemistry, University of South Florida, 4202 E Fowler Ave., Tampa, FL, USA*

[c] *School of Polymer Science and Engineering, Center for Optoelectronic Materials and Devices, The University of Southern Mississippi, Hattiesburg, MS, 39406, United States.*

[d] *Department of Electrical and Computer Engineering, Center for Materials for Information Technology, The University of Alabama, Tuscaloosa, AL 35487, United States*

[e] *Department of Physics and Astronomy, Department of Chemistry Mississippi State University, Mississippi State, MS 39762*

[1] *These authors contributed to the work equally*

Corresponding authors: jianfengcai@usf.edu and qilin.dai@jsums.edu

Abstract

Perovskite solar cells (PSCs) exhibited remarkable progress for small aperture area cells, however, the performance of its counterpart, large aperture area cells, lags due to non-uniform and defective perovskite layers. Here, we fabricate reproducible large area homogeneous perovskite films at room temperature and without controlling humidity (up to 40% RH) with a slot die coater on a c-

TiO_2 layer deposited using a large area chemical bath. A new artificial peptide – sulfonyl-γ-AA peptide (F-GLU-S) was employed to modify the slot-die coated perovskite surface, grain boundaries and electronic defects. The multi-functional F-GLU-S with carbonyl, carboxyl, sulfonyl, benzene, and chloro groups was capable of strongly interacting with the perovskite layer and repairing the uncoordinated Pb^{2+} ions and halide vacancies. As a result, both the electron and hole densities of defects were significantly suppressed; consequently, the non-radiative recombination was effectively suppressed for the modified device which can be explicitly seen in the device performance where both V_{oc} and FF of the modified device improved considerably. Therefore, F-GLU-S modified slot-die coated $MAPbI_3$ – based devices demonstrated outstanding performance of 21.44% PCE with a V_{oc} of 1.13V, J_{sc} of 24.64cm^{-2}, and FF 76.99%. Moreover, passivation impeded the infiltration of moisture and oxygen due to its hydrophobic nature and defect repair potential. As a result, the modified device retained above 92% of its original PCE after 720 h in air (room temperature and 40-60% RH).

Keywords: Slot-die coating, γ-AApeptide, defects, amino acid passivation, chemical bath deposited c-TiO_2, perovskite powder

Introduction

The power conversion efficiency (PCE) of PSCs has increased dramatically in the last decade and a certified PCE of above 25% has been recorded for the small aperture area cells.[1] This progress demonstrates the potential of PSCs to be the next generation energy alternative. Now the primary task to commercialize PSCs is to design efficient scale up techniques to fabricate large area perovskite devices (modules) with equivalent PCE as a small aperture area cell. Currently, most of the devices with high PCE are small area cells and prepared by the commonly employed spin-coating.[1-2] However, spin-coating techniques do not deliver homogeneous films over large area

as the quality deteriorates with increasing substrate area and less favorable to prepare modules.[3] The largest sub-module prepared by spin-coating of $MAPbI_3$ delivered a maximum PCE of only 12.6%.[4] Therefore, alternative film processing techniques have been developed to realize homogeneous perovskite films over large area including slot-die coating, blade-coating, bar-coating, thermal deposition, ink-jet printing, and spray-coating.[5-10] Among all of these techniques, the slot-die coating demonstrated higher yield and reproducibility due to the continuous and uninterrupted precursor supply and precise control of coating parameters, respectively.[11] Intriguingly, slot-die coating could directly integrate to the roll-to-roll and sheet-to-sheet process.[12]

With respect to demonstrating large area PSCs with slot-die coater, various perovskite inks were slot-die coated to fabricate PSCs and modules. Ehsan Rezaee et al. slot-die coted $MAPbI_3$ and the device delivered a maximum PCE of 17.4% (aperture area=0.25cm^2).[13] Similarly, slot-die coated $MAPbI_3$ on ITO/SnO_2 exhibited 18% PCE (aperture area=0.06cm^2).[11] Slot-die coated $Cs_{0.05}MA_{0.4}FA_{0.55}$ $Pb(I_{0.96}Br_{0.04})_3$ produced 19% PCE for small area cell.[14] Moreover, MAI free slot-die coated $Cs_{0.16}FA_{0.84}Pb(I_{0\cdot88}Br_{0.12})_3$ demonstrated 18% PCE (aperture area= 0.09 cm^2).[15] However, the slot-die coating process is controlled by a machine, realizing homogeneous film requires tedious optimizations to achieve uniform perovskite crystallinity and morphology over large areas. In the slot-die coated perovskite, the homogeneity of the film is influenced by several factors such as precursor viscosity, coating speed, perovskite flow rate, coating gap, coating temperature, surface tension, meniscus stability, and post-annealing temperature. Moreover, the uniformity of the bottom c-TiO_2 layer influenced the homogeneity of the slot-die coated perovskite. Recently, scalable chemical bath deposition was employed to prepare large area SnO_2 electron transport layer (ETL) on which mixed perovskite was slot-die-coated the device demonstrated 19.2% PCE (aperture area= 0.09 cm^2).[16] The PCE of slot die coated PSCs are highly influenced by the

perovskite crystallinity and morphology. In general, the polycrystalline perovskite film contains high concentration of structural and electronic defects which impedes the device to attain the highest theoretically predicted PCE. These defects could be antisite, uncoordinated Pb^{2+}, uncoordinated halide, cation vacancies, halide vacancies, and Pb clusters, or a mixture of these defects, which trigger non-radiative recombination resulting in substantial photogenerated carrier loss. Additionally, the defects could trigger undesirable hysteresis and may influence the charge transport and extraction which results in inferior performance. Furthermore, the defects at the surface and grain boundaries are a pathway to ion migration that causes series device degradation. Recently, 4-fluoro-phenethylammonium iodide (4-F-PEAI) and poly (9-vinylcarbazole) (PVK) were added in $FAPbI_3$ and antisolvent solution, respectively to improve crystallinity, suppressed defects and trap sites, and repressed ion migration, as a result, the passivated device demonstrated 21.6% PCE.[17] Therefore, it is necessary to passivate the slot-die coated perovskite film to suppress defects, enhance PCE, and extend the long-term stability of the devices.[17-19] In general, to fabricate efficient large area perovskite cells, it not only requires smooth, homogeneous, pinhole-free perovskite layers but also it needs a suppressed electronic defects as well. The defect density of slot-die coated perovskites can be suppressed by additive engineering of the perovskite precursor solution[20], by post-surface passivation of the polycrystalline perovskite film,[21] or by modifying the interface of perovskite with electron or hole transporting layers.[22] Considering these approaches, recently few passivation molecules and additives were incorporated to modify the perovskite growth, crystallization, morphology, and defects. Minyong Du modified the surface of slot-die prepared $FA_{0.91}Cs_{0.09}PbI_3$ by an ionic liquid $[M_4N]BF_4$ to decrease the surface defect density and carrier recombination.[21] The crystal quality and morphology of slot-die coated $MAPbI_3$ was modified by added potassium thiocyanate (KSCN).[20] Similarly, 2-hydroxyethyl acrylate

(HEA) was added to $Cs_{0.175}FA_{0.750}MA_{0.075}Pb(I_{0.880}Br_{0.120})_3$ to modify the perovskite growth and defects.[23] Moreover, nonvolatile Lewis base diphenyl sulfoxide (DPSO) was added to the MA-free $FA_{0.83}Cs_{0.17}PbI_{2.83}Br_{0.17}$ to slow the crystallization of perovskite during the slot-die coating process.[24] Likewise, $CsPbBr_3$ and KPb_2Br_5 were added to the $Cs_{0.15}FA_{0.85}Pb(I_{0.83}Br_{0.17})_3$ ink to modify the perovskite crystallization.[25] Furthermore, Jinzhao Li et al. employed a strongly coordinating solvent, DMSO, with $MAPbI_3$, where the DMSO suppressed the intermediate phase formed during slot-die process and enhanced the perovskite morphology.[18]

Furthermore, various passivation molecules were established to passivate halide vacancies[26-30], cation vacancies,[27,31-34] and both halide and cation vacancies of the perovskite film.[18,35-44] Recently, amino acid based molecules have received attention to passivate the perovskite layer and/or to modify the interface because of the amino acid structure comprises multi-functional groups such as carboxyl and amino, which can strongly interacted with the perovskite film to potentially passivate both positively and negatively charged defects.[40,45-56] Recently, $FA_{0.65}MA_{0.35}PbI_{3-\delta}Cl_{\delta}$ perovskite defects were substantially suppressed with a KKK-type M13. It was synthesized from lysine and wild virus and exhibited strong interaction with the perovskite; as a result, the defects significantly repressed and a PCE of 23.6% was achieved for spin-coated small aperture area device.[51] Similarly, p-aminobenzoic acid iodide (PABA·HI) was employed to modified $MAPbI_3$ defects where both the amino group and the carboxylic acid group in PABA·HI interacted with the Pb-I through hydrogen bonds and successfully passivated the trap density of states.[45] We recently developed a class of peptidomimetics – sulfonyl-γ-AApeptide, which possess tremendous potential of chemodiversity, well-defined folding propensity, as well as remarkable stability.[57-59] Herein, we present the passivation of slot-die coated $MAPbI_3$ layer with an amphiphilic sulfonyl-γ-AApeptide - F-GLU-S. The sulfonyl-γ-AApeptide was designed to bear both hydrophobic and

hydrophilic groups. Its "hydrophobic nature" occurs after the self-assembly process (passivation), i.e., after the hydrophilic carboxylic acid is combined with lead, the hydrophobic portion of the molecule is exposed to the outermost interface to help the perovskite resist water in the environment. Particularly, the molecule is comprised of benzene, carboxyl, carboxylic acid, amino, sulfonyl, and chloro functional groups which form strong interactions with the perovskite to significantly suppress both cationic and halide vacancies. As a result, the slot-die coated perovskite device exhibited a champion performance of 21.44% PCE. Moreover, F-GLU-S modified device exhibited excellent moisture stability compared to the control device. This study will open a new avenue in the synthesis of amino acid-based molecules to modify the perovskite films for decent PCE and stability.

Experimental Section

Materials: Fluorine tin oxide (FTO) substrates were purchased from Youxuan TECH, China. $TiCl_4$ bought from Alfa Aesar. Lead iodide (PbI_2) was purchased from TCI. Methylammonium iodide (MAI) was purchased from Xi'an Polymer Light Technology Corporation (China). 2,2′,7,7′-Tetrakis [N,N-di (4-methoxyphenyl)amino]-9,9′-spirobifluorene (Spiro-OMeTAD) and FK 209 Co(III) Li TFSI salt were purchased from Sigma-Aldrich. Lithium bis(trifluoromethanesulfony)imide (Li-TFSI) from TCI. 4-tert-butylpyridine (4-tBP) and were purchased from Accela. FK209 Co (III) Li-TFSI obtained from Greatcell materials. Poly[bis(4-phenyl)(2,4,6-trimethylphenyl)amine] (PTAA) was obtained from Solaris Chem (Canada). [6,6]-phenyl C61-butyric acid methyl ester ($PC_{61}BM$) were purchased from Sigma-Aldrich. N,N-Dimethylformamide (DMF), isopropanol (IPA), diethyl ether (EE), acetonitrile (ACN) and chlorobenzene (CB) were purchased from Sigma-Aldrich. Dimethyl sulfoxide (DMSO) and gold

bar (Au 99.998%) were purchased from Alfa Aesar. F-GLU-S synthesized in our lab. All chemicals were used as received without further treatment.

Device fabrication: The FTO substrate cleaned according to literature.[60] The c-TiO_2 prepared by water bath technique where UV-Ozone treated 10×10cm^2 FTO substrate was immersed in iced aqueous $TiCl_4$ solution at 70ºC for 45 min. The thickness of the c-TiO_2 layer controlled by immersion time. Next, the substrate rinsed with copious amount of water and ethanol to remove the physiosorbed particles, subsequently, the substrate annealed at 200ºC for 30min.

The slot die perovskite ink is prepared as follows by modifying literature report.[61] Firstly, we synthesized $MAPbI_3$ powder in air (fume hood) at room temperature and without controlling humidity. 1.28g of MAI added into 28mL acetonitrile (ACN) and stirred for 10 min. Then, 3.69g of PbI_2 added to the MAI solution, at this stage spontaneous black perovskite was formed. To ensure the complete perovskite formation the stirring continues for 2h. Then, the perovskite powder filtered and washed wish ACN and EE until the supernatant became colorless immediately followed dried the powder in vacuum oven at 70ºC for 2h. Secondly, the perovskite ink was prepared by reacting 3g of the synthesized $MAPbI_3$ black powder to 10 mL of methylamine (MA) gas for 4h in sealed container, where the MA gas diffused to the perovskite powder and formed yellow viscos perovskite ink. To facilitate the reaction, we stirred both the perovskite powder and MA gas solution at slow speed. Lastly, the slot-die $MAPbI_3$ precursor solution is prepared by mixing the viscus perovskite ink and acetonitrile (1:1 v/v).

The perovskite was slot-die coated by infinityPV RLC in air glovebox up to 40% RH. The perovskite film and device didn't exhibit significant difference when the humidity is 10%-40%, however, for above 40% RH the device showed poorer performance. To reduce the humidity in the air glovebox to the desired humidity (in our experiment 30 % RH), we blew dry air. Then, the

perovskite was slot-die coated on large area c-TiO_2 at a coating speed of 0.07m min^{-1} with a perovskite flow rate of 0.07ml min^{-1} at a coating gap of 100 µm at room temperature. Then, the perovskite film annealed at 100ºC for 10min. To test the influence of surface passivation on device performance we cut the large area perovskite layer to 1.5×1.5cm^{-2} size. After that, the passivation layer prepared by spun-coat 2mM F-GLU-S in 2-propanol at 4000rpm for 30s. The modified perovskite film then annealed at 70ºC for 10min. Once the passivated layer cooled down, spiro-OMeTAD hole-transport layer is prepared following literature.[62] Finally, 80nm Au layer prepared by thermal deposition.

Film and device characterizations: The perovskite and modified perovskite films were characterized by FT-IR, XRD, 2D-GIWAXS, XPS, UV-Vis, SEM, AFM, PL, TRPL, I-V, EQE, and EIS using the instruments described in reference.[62]

Results and discussion

First, we prepared homogenous large area c-TiO_2 by a chemical bath method (CBM) at low temperature. To fabricate efficient large area n-i-p PSCs, the electron transport layer (ETL) should be homogenous and pinhole free – if not the electron extraction and transport are negatively influenced.[16,60] Recently, Iwan Zimmermann et al. demonstrated the preparation of large area SnO_2 by CBM.[16] Here, as illustrated in Scheme 1a, we prepared uniform and pinhole free large area (10×10cm^2) c-TiO_2 from iced aqueous $TiCl_4$ solution. The UV-ozone cleaned FTO substrate was immersed in the solution for 45 min at 70 °C. Subsequently, the substrates were rinsed with DI water and ethanol followed by annealing at 200 °C for 30 min where ~40 nm smooth c-TiO_2 was achieved. The thickness of c-TiO_2 was controlled by immersion time and concentration. Next, the perovskite film was slot-die coated on the large area UV-ozone cleaned c-TiO_2 layer. The perovskite solution preparation and slot-die coating parameters are briefly explained in

experimental section. The slot-die prepared large area ($10\times10cm^2$) perovskite film morphology and crystallinity are primary influenced by the type of solvent employed to prepare perovskite precursor solution as it controls the film coating and drying process. Here we employed the high vapor pressure and low evaporation temperature acetonitrile-based perovskite precursor solution to achieve a homogenous perovskite layer by slot-die coating at room coating temperature (21-24 °C). The flow rate, coating gap, and coating speed thoroughly were optimized to get homogenous perovskite layers. A narrow coating gap (~100 μm) and low coating speed of 0.07m min^{-1} delivered highly smooth and crystalline perovskite layer. Subsequently, we modified the slot-die coated perovskite by spin-coating 2mM γ-AApeptide F-GLU-S in 2-propanol. The post surface passivated slot-die coated perovskite layer and F-GLU-S molecule are illustrated in Scheme 1b. The amphiphilic sulfonyl-γ-AApeptide was designed to bear both hydrophobic and hydrophilic groups. Its "hydrophobic nature" occurred after self-assemble process (passivation); after the hydrophilic carboxylic acid is combined with lead, the hydrophobic portion of the molecule will be exposed to the outside to help the perovskite resist water in the environment. Particularly, F-GLU-S is comprised of carbonyl, carboxyl, amino, sulphonyl and chloro groups, which are expected to have strong interactions with the perovskite to modify defects. The -COOH and NH of the F-GLU-S interacted with the Pb-I perovskite framework through hydrogen bonding and suppressed anionic and cationic defects, respectively.[40,45] Moreover, the C=O of the F-GLU-S coordinated with the uncoordinated Pb^{2+} ions, as a result, F-GLU-S could effectively passivate both anionic and cationic defects. The interaction of F-GLU-S and slot-die coated $MAPbI_3$ is illustrated in Scheme 1c.

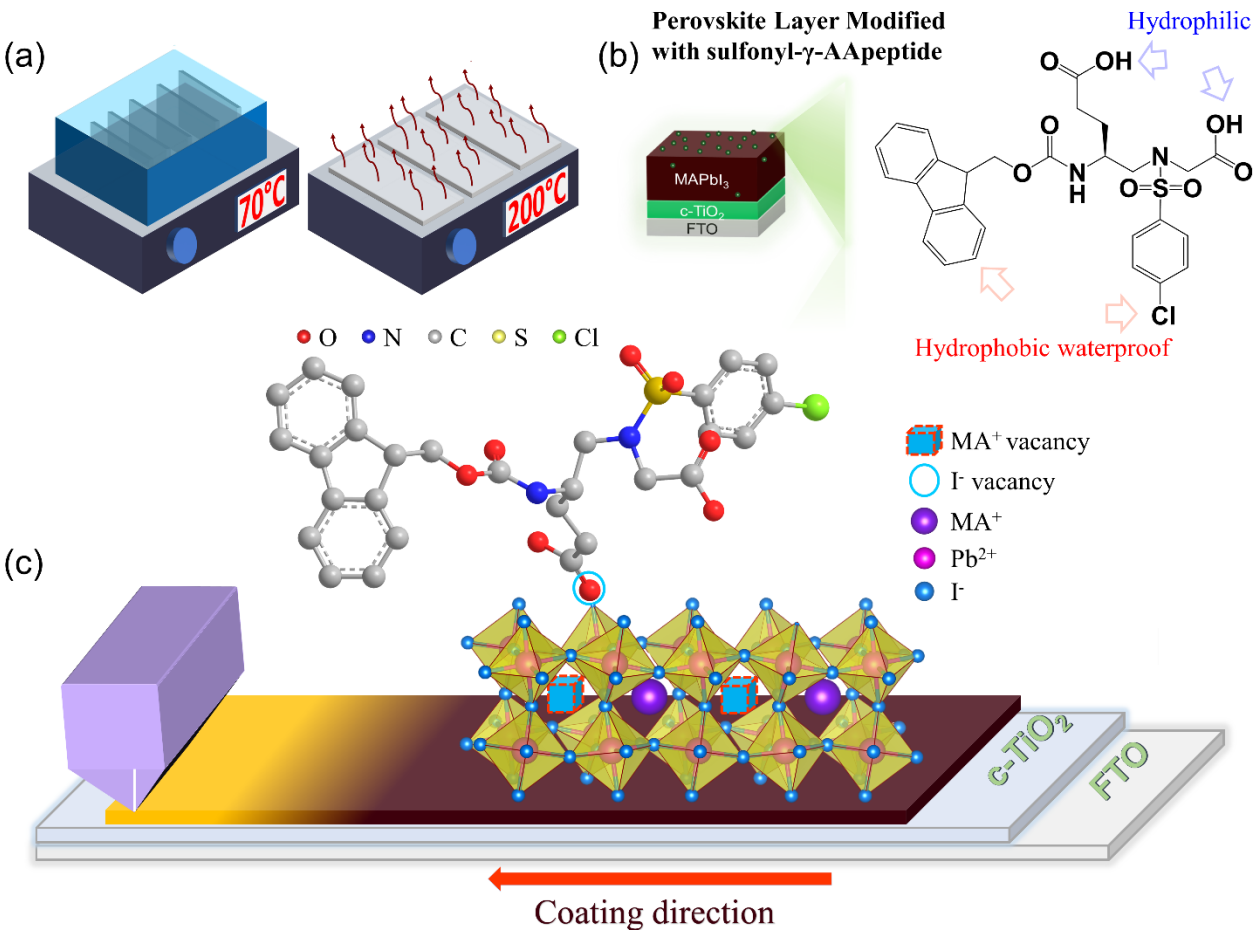

Scheme 1. Schematic illustration of (a) c-TiO_2 preparation by chemical bath method, (b) perovskite film passivation by F-GLU-S and molecular structure of F-GLU-S, and (c) interaction of F-GLU-S with $MAPbI_3$ perovskite.

To understand the interaction between F-GLU-S and slot-die coated perovskite, we first investigated with Fourier transform infrared spectroscopy (FTIR). The FTIR peak at 1661 cm^{-1} is assigned for C=O of the F-GLU-S; this peak is significantly shifted to 1713cm^{-1} when employed as a passivation layer clearly demonstrating the C=O coordinated with the uncoordinated Pb^{2+} ions and modified the perovskite defects (Figure 1a). The FTIR of the control, F-GLU-S modified perovskite, and F-GLU-S powder is provided in Figure S1, where the incorporation of F-GLU-S is further verified with the presence of additional peaks at from 620-1500cm^{-1}. Then, we recorded

the XRD of the control and F-GLU-S modified slot-die coated perovskite films in which both films exhibited very sharp peaks at (110), (220) and (224) without any significant difference (Figure 1b). To further understand the crystallinity and phase of the control and F-GLU-S modified slot-died coated perovskite films, we record 2D grazing incidence wide angle x-ray spectroscopy (2D-GIWAXS) where we found that the slot-die coated perovskite exhibited extraordinary crystallinity this was particularly observed for the F-GLU-S modified perovskite. The GIWAXS and Q Vector comparison of the control and F-GLU-S modified $MAPbI_3$ are provided in Figure 1c-f. The 2D-GIWAXS image exhibited formation of a mixture of many bright rings and bright spots. The bright scattering spots come from the ordered crystal structure and have the same orientation relative to the substrate. The scattering rings come from the disoriented crystal structure, which might locate at the interface. We have observed similar crystallinity as the scattering intensities from the two samples are close (Figure e) with the same exposure time and sample thickness. The anisotropic sharp scattering points and corresponding isotropic scattering rings indicate that majorly well-oriented crystalline perovskites were formed by the slot die coating. Additionally, the peaks are sharp which implies the perovskite grains are very large. Furthermore, we have clearly observed the presence of minute peak for the control sample at 0.895Å (Figure 1e-f) which shows the presence of uncoordinated PbI_2 in the film which corroborated with the FTIR result. The PbI_2 peak is eliminated for the modified perovskite which implies that the F-GLU-S interacted with $MAPbI_3$ and effectively suppressed the uncoordinated Pb^{2+} (Figure 1e-f).

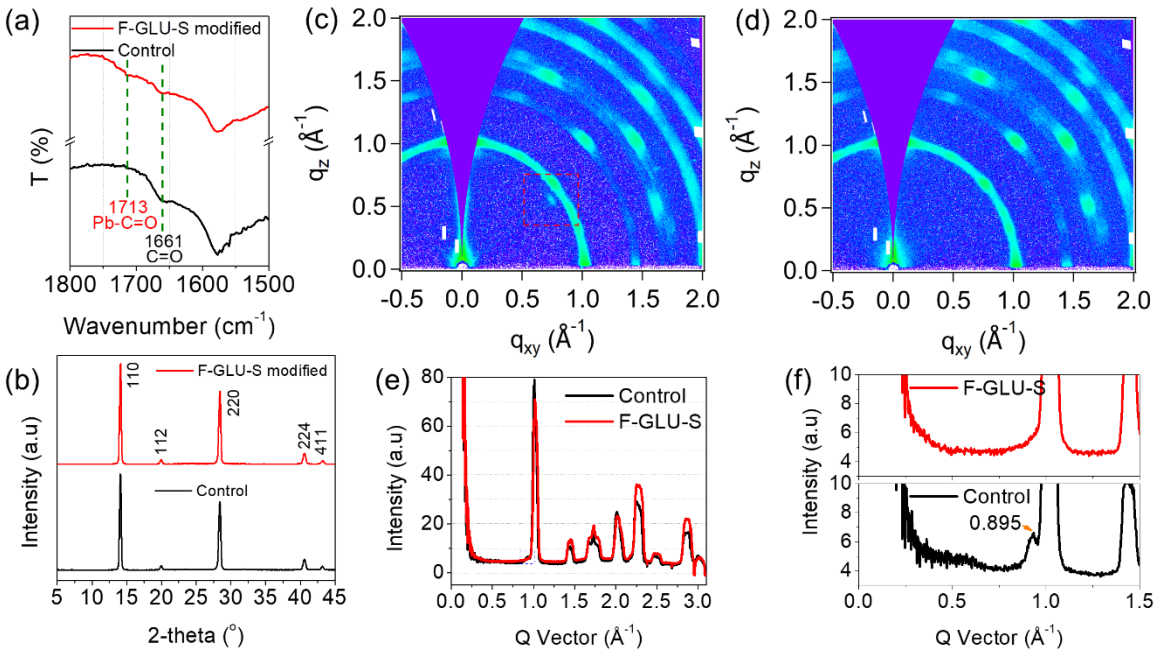

Figure 1. Characterization of the interaction between $MAPbI_3$ and F-GLU-S. (a) FTIR spectra of the control and 2mM F-GLU-S modified $MAPbI_3$, (b) XRD of the control and 2mM F-GLU-S modified $MAPbI_3$, (c) GIWAXS of the control perovskite, (d) GIWAXS of the modified perovskite, (e) Azimuthally integrated intensity profiles of the 2D-GIWAXS patterns of the control and F-GLU-S modified $MAPbI_3$, and (f) Zoomed azimuthally integrated intensity profiles of the control and F-GLU-S modified $MAPbI_3$. The small spot at 0.895Å for the control sample is corresponding to the red rectangle in Figure 1c which clearly showed the presence of uncoordinated Pb^{2+} in the control perovskite.

We further employed X-ray photoelectron spectroscopy (XPS) to investigate the chemical composition changes of C1s, Pb4f, O1s, N1s, I3d, Cl2p and S2p for slot-die coated $MAPbI_3$ films with and without F-GLU-S modification. We calibrated the C-C peak at 284.84 eV for both the control and F-GLU-S modified perovskite films to compare the XPS peak changes.[63] The Cls spectra are shown in Figure 2a and Figure S2 (a-b). F-GLU-S is organic, thus the C/Pb ratio

increases significantly for the modified perovskite film confirming the presence of F-GLU-S on the surface and grain boundaries of the

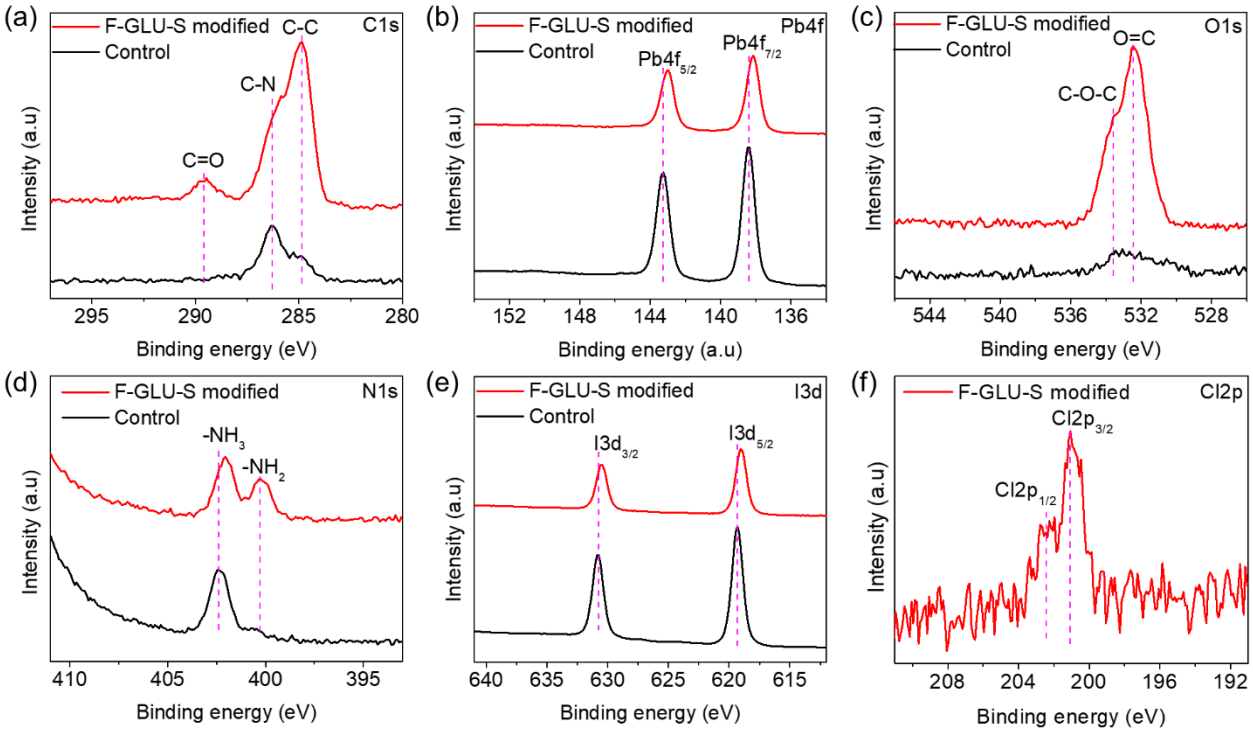

Figure 2. High-resolution XPS spectrum of the control and 2mM F-GLU-S modified $MAPbI_3$ films. (a) C1s, (b) Pb4f, (c) O1s, (d)N1s, (e) I3d, and (f) Cl2p.

perovskite layer. The peak at 286.35 eV in the control perovskite is assigned to C-N from $MAPbI_3$, which is shifted to 286.08 eV for the modified perovskite.[64] More importantly, the F-GLU-S modified perovskite exhibited an additional significant peak at 289.59 eV which is assigned to C=O from the carbonyl group of the F-GLU-S, confirming the presence F-GLU-S on the treated perovskite.[65]

Figure 2b shows the Pb4f spectra where the two Pb4f peaks at 143.12 eV and 138.42eV for the control perovskite are assigned to $Pb4f_{5/2}$ and $Pb4f_{7/2}$, respectively, which are shifted to 142.99 eV and 138.14 eV, respectively, for the F-GLU-S modified $MAPbI_3$, clearly indicating the interaction

between $MAPbI_3$ and F-GLU-S.[63] Figure 2c shows the O1s XPS peak for the control and F-GLU-S passivated perovskite. We clearly observed two O1s peaks at 532.46 eV (O=C) and 533.54 eV (C-O-C) for the control and modified perovskite. Due to the additional O from -COOH and C=O in the modified perovskite, the O/Pb ratio significantly increased for the modified F-GLU-S perovskite.[53]

The N1s spectra are presented in Figure 2d, where the control perovskite exhibited a single peak at 402.44 eV which is assigned for $-NH_3$ arising from the $MAPbI_3$. This N1s peak is shifted to a lower binding energy of 402.04 eV for the F-GLU-S treated perovskite.[63] Additionally, the modified perovskite exhibited an extra peak at 400.29 eV assigned for $-NH_2$ originating from F-GLU-S. These shifts in N1s peaks are attributed to the interaction between F-GLU-S and the perovskite. The I3d spectra are shown in Figure 2d, where the two main peaks at 630.83 eV and 619.31 eV are assigned to I $3d_{3/2}$ and $I3d_{5/2}$ for the control slot-die coated perovskite film which are shifted to lower binding energy of 630.48 eV and 619.01 eV, respectively for F-GLU-S modified perovskite. Additionally, F-GLU-S modified perovskite exhibit Cl2p (Figure 2f) and S2p (Figure S3c) peaks which are not present for the control perovskite film confirming the strong interaction between F-GLU-S and perovskite layer and the presence of F-GLU-S at the surface of the modified film. The Cl2p spectra has two main peaks at 202.42 eV ($Cl2p_{1/2}$) and 201.08 eV ($Cl2p_{3/2}$). Likewise, the S2p has two main peaks at 169.68 eV (Sp1/2) and 168.57 eV ($Sp_{3/2}$). The full XPS spectra of the control and F-GLU-S modified perovskite is presented in Figure S2d. The binding energy shifts associated with C1s, Pb4f, O1s, N1s, and I3d and the emergence of Cl2p and S2p by F-GLU-S signifies the interaction between F-GLU-S and perovskite suggesting the passivation of perovskite to suppress the density of traps. The XPS investigation validated the FTIR and 2D-GIWAXS results.

Figure 3a-b and Figure S3a-b demonstrated the top view SEM image of the control and F-GLU-S modified films where both exhibited highly compact and homogenous layers without significant morphology difference which implies the perovskite crystallization may not considerably alter with post-passivation of perovskite layer with F-GLU-S. Previous studies of amino acid based passivation molecules modified the perovskite crystallization when applied in bulk perovskite precursor.[56] Intriguingly, the pinholes on the control slot-die coated perovskite decreased when the surface was modified with F-GLU-S (Figure 3Sa-b). The AFM phase amplitude, topography, and 3D images of the control and F-GLU-S modified perovskites are provided in Figure S4.

After we confirmed the successful interaction between F-GLU-S and perovskite, we investigated the influence of F-GLU-S on the optoelectrical property perovskite. The UV-vis spectra of the control and 2mM F-GLU-S modified $MAPbI_3$ film are provided in Figure S5, where the absorption onset of the perovskite is not altered signifying the F-GLU-S modification did not shift the energy level or bandgap of the perovskite. Moreover, to show the uniformity of the perovskite film over a large area, we fabricated 10×10 cm^2 perovskite film by slot-die coater (Figure S6a) and cut into sixteen 2.5×2.5 cm^2 and investigated their UV-Vis absorption. The absorption spectra are presented in Figure S6b, where the UV-Vis of all the perovskite layers overlapped which demonstrated uniform film was achieved over the entire area.

The influence of F-GLU-S on charge extraction was investigated with steady-state photoluminescence (PL) and time-resolved PL (Figure 3c-d). The control and modified perovskite layers were prepared by slot-die coating on the glass substrate and the light is guided from the perovskite side. The PL of the F-GLU-S modified perovskite exhibited substantial PL improvement which indicates substantial suppression of the non-radiative recombination on the surface and grain boundaries of the modified perovskite film.[62,66]

The lifetime of carriers of the control and F-GLU-S modified perovskite are measured by the time-resolved PL and fitted using equations (1) and (2).

$$Y = A_1 \exp\left(\frac{-t}{\tau_1}\right) + A_2 \exp\left(\frac{-t}{\tau_2}\right) \qquad \text{equation (1)}$$

$$\tau_{avg} = \frac{A_1 {\tau_1}^2 + A_2 {\tau_2}^2}{A_1 \tau_1 + A_2 \tau_2} \qquad \text{equation (2)}$$

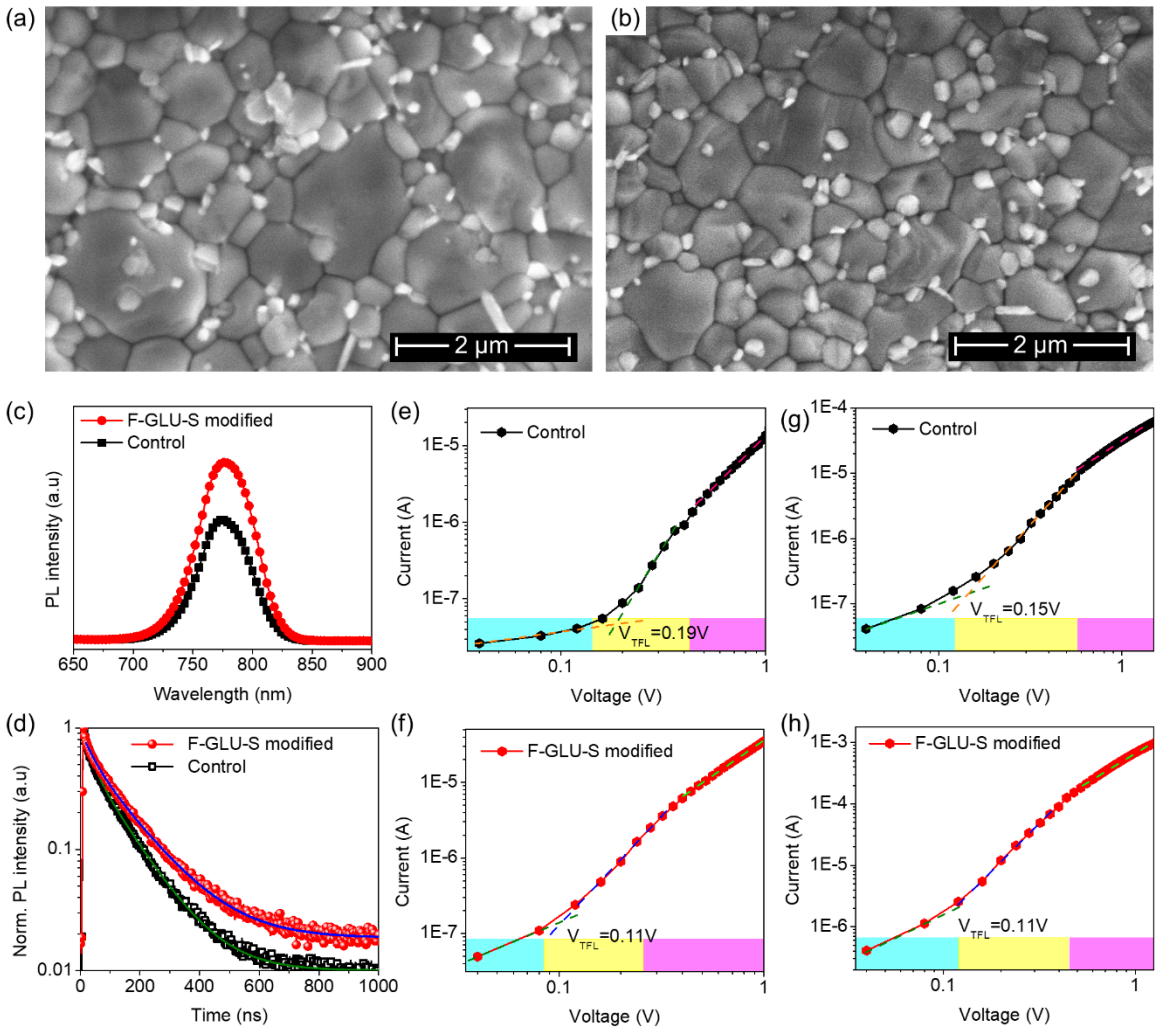

Figure 3. (a) SEM image of control perovskite, (b) SEM image of F-GLU-F modified $MAPbI_3$, (c) Steady-state PL of the control and 2mM F-GLU-S modified $MAPbI_3$ on glass. (d) TRPL of the control and 2mM F-GLU-S modified $MAPbI_3$. (e-f) Electron-only device with a structure of

316 FTO/c-TiO_2/ $MAPbI_3$ (with and without 2mM F-GLU-S)/PCBM/Au, (g-h) Hole-only device
317 with a structure of FTO/PEDOT:PSS/ $MAPbI_3$ (with and without 2mM F-GLU-S)/Spiro-
318 OMeTAD/Au.

319 A_1 and A_2 are the relative amplitudes, t is time, τ_1 and τ_2 are the lifetime values for the fast and
320 slow decay, respectively.

321 The average lifetime of the control slot-die coated perovskite film is 44.42 ns, which increased to
322 54.88 ns for the F-GLU-S modified perovskite implying that defects are suppressed with F-GLU-
323 S modification. The lifetime results are summarized in Table S1. Based on the interaction of F-
324 GLU-S and perovskite and the morphology study, the F-GLU-S suppressed both the electronic
325 defects through eliminating non-recombination centers and surface defects by modifying the
326 surface and grain boundary defects. Consequently, a superior PL was obtained for the modified
327 film.

328 To quantify the electron and hole traps, we fabricated electron-only and hole-only devices for the
329 control and F-GLU-S modified device, respectively. The electron-only devices are fabricated with
330 a structure of FTO/c-TiO_2/$MAPbI_3$ (with and without F-GLU-S)/PCBM/Au. The device is
331 measured at dark condition and the number of defects are calculated according to equation 3, where
332 ε is the relative dielectric constant of $MAPbI_3$ (ε=32), [67-68] ε_0 is vacuum permittivity, V_{TFL} is trap-
333 filled limit voltage, e is the elementary charge, and L is the thickness of $MAPbI_3$ with and without
334 F-GLU-S and N_{traps} is the number of traps.

335 $$N_{traps} = \frac{2\varepsilon\varepsilon_0 V_{TFL}}{eL^2} \qquad \text{equation (3)}$$

336 The double logarithmic graph of the control and F-GLU-S modified electron-only devices are
337 given in Figure 3e-f. The calculated N_{traps} for the control device exhibited $3.47\times10^{15}cm^{-3}$. Up on

F-GLU-S treatment the N_{traps} substantially reduced by 49% to $1.83\times10^{15}cm^{-3}$. Subsequently, we fabricated the hole-only device with a structure of FTO/PEDOT:PSS/$MAPbI_3$ (with and without F-GLU-S)/Spiro-OMeTAD/Au is to quantify the number of hole traps (Figure 3g-h). The control hole-only device exhibited $3.05\times10^{15}cm^{-3}$ N_{traps}, intriguingly, the N_{traps} minimized to $2.24\times10^{15}cm^{-3}$ for F-GLU-S modified devices. The electron and hole N_{traps} results revealed F-GLU-S suppressed both cationic and anionic defects from the perovskite which ultimately reduce the non-radiative recombination significantly to improve the device V_{oc} and FF. The N_{traps} study is consistent with the PL study. Full SCLC parameters are summarized in Table S2.

The interface between perovskite and spiro-OMeTAD plays crucial role for charge transfer. First, we employed kelvin probe force microscopy (KPFM) to study the contact potential differences of the perovskite films with and without F-GLU-S (Figure S7). The contact potential differences of perovskite film increase from *ca.* 157 mV to *ca.* 286 mV, which shows significant potential in the carrier transport in the devices and enhanced V_{oc} of the devices.[18,69] Moreover, we studied ultraviolet photoelectron spectroscopy (UPS) to quantify the energy level alignment of the perovskite layer with and without F-GLU-S treatment (Figure S8a-c). The control $MAPbI_3$ exhibited a valence band of -5.40 eV which is consistent with the previous study.[70] Upon F-GLU-S modification the valence band shifted to -5.54 eV,[45] which is beneficial to minimize the recombination of electrons and holes at the interface.[71]

Next, to evaluate the significance of F-GLU-S on the device performance, we fabricated PSCs with a structure of FTO/c-TiO_2/$MAPbI_3$ (with and without F-GLU-S)/Spiro-OMeTAD/Au (Figure 4a). Initially, we fabricated the control slot-die coated perovskite device with the optimized fabrication process discussed in experimental section. The control device demonstrated a maximum PCE of 19.10% with a J_{sc} of a V_{oc} of 1.104V, $24.40mAcm^{-2}$, and FF of 70.90% in reverse

bias, and a forward bias PCE of 17.46% with a J_{sc} of 24.19 $mAcm^{-2}$, V_{oc} of 1.110 V and FF of 65.01%, as a result, the control device exhibited a significant hysteresis index (HI) of 0.086 calculated by $HI=(PCE_{reverse}-PCE_{forward})/PCE_{reverse}$.[43] First, we spin-coated 30µL absolute 2-propanol on the perovskite layer to study the impact of 2-propanol on device performance, however, 2-propanol couldn't influence the morphology of the perovskite layer and device performance.[72] Then, various concentrations of F-GLU-S in 2-propanol (0mM, 0.5mM, 1mM, 2mM and 3mM) were spin coated on the slot-die coted perovskite layer to optimize the best concentration. The concentration optimization is summarized in the box chart in Figure S9, where at small F-GLU-S concentration (0.5-1mM), the V_{oc} of the modified device improved but was not reproducible. At higher concentration (3mM), the bulky F-GLU-S on the surface induces charge resistance as a result both J_{sc} and FF of the modified device decreased. The 2mM F-GLU-S concentration delivered impressive photovoltaic parameters where all the J_{sc}, V_{oc} and FF improved, and importantly the results were reproducible. Consequently, the F-GLU-S modified perovskite produced outstanding performance of 21.44% PCE with a V_{oc} of 1.130V, a J_{sc} of 24.64$mAcm^{-2}$, and FF of 76.99% at reverse bias which is one of the best performances amongst the modified slot-die perovskite device with various passivation/additive molecules (Table S3). Intriguingly, the F-GLU-S device demonstrated a forward bias PCE of 20.94% with a J_{sc} of 24.37 $mAcm^{-2}$, V_{oc} of 1.130 V and FF of 76.03% with reduced HI of 0.023. The HI results validated that defects are effectively reduced by F-GLU-S treatment. The champion I-V curve for the control and F-GLU-S modified perovskite is provided in Figure 4b. Next, we measured the stabilized PCE of the control and F-GLU-S modified $MAPbI_3$ based device at maximum power point of 0.98 V for 150s (Figure 4c). The control device power out decreased significantly from 19.10% PCE to 15.95% in 150s which could be associated with an increase in the concentration of defect density of states while

384 measurement (such as ion diffusion) that leads to severe recombination as a result the PCE
385 deteriorated over time.[73] Interestingly, the modified devices demonstrated stable stabilized power
386 output over the measurement time that suggested the defects are effectively suppressed (no
387 significant recombination) which is consistent with the PL and SCLC study. Moreover, F-GLU-S
388 effectively modified the interface between perovskite and spiro-OMeTAD (doped with Li-TFSI
389 and TBP). However, in the control device, the Li^+ could migrate to the and perovskite/spiro-
390 OMeTAD interface that resulted severe recombination in the device which declined PCE over
391 time.[73] This result implies the F-GLU-S not only improved the device performance, but it also
392 substantially improves the stability of the working device.

393 To check the reproducibility of our results, we fabricated 20 devices each for the control and F-
394 GLU-S modified slot-die coted perovskite and the results summarized on the box chart in Figure
395 4d-g. The results demonstrated that F-GLU-S treated slot-die coated perovskite exhibited
396 substantial improvements on both V_{oc} and FF which validates the potential of F-GLU-S to repress
397 the surface, grain boundary and electronic defects which corroborated the results of PL, TRPL,
398 hole-only and electro-only device. The F-GLU-S coordinated with the perovskite through Lewis
399 acid-base coordination (Pb-C=O) to suppress the uncoordinated Pb^{2+} ions and also formed
400 hydrogen bonding through chloro functional group where the Cl^- could directly substitute the I^-
401 vacancy. As a result, the electronic defects substantially reduced which leads to improved PL
402 device performance for the F-GLU-S modified device. Moreover, to study the uniformity of slot-
403 die coated perovskite over a large area we fabricated large area (1.12 cm^2) perovskite devices
404 (Figure S10). Intriguingly, the large area device demonstrated a champion PCE of 15.72% with a
405 J_{sc} of 24.47cm^2, a V_{oc} of 1.09 V, and an FF of 58.93%. It has been reported that in the large area
406 cells the performance loss is due to large series resistance (R_s), which drastically lowers the fill

factor.[74] The R_s increasing with aperture area. Subsequently, we recorded the external quantum efficiency (EQE) of the control and F-GLU-S modified devices (Figure 4h), where the integrated J_{sc} of 19.85 $mAcm^{-2}$ and 20.16 $mAcm^{-2}$ was measured for the control and F-GLU-S -modified device, respectively. The discrepancy between the integrated J_{sc} and the J_{sc} measured in the I–V curve arises because the EQE measurement is carried out in a single wavelength with considerably lower intensity than the one sun radiation.[75] These deviation might result from also due to the nonlinear recombination mechanism in the devices.[75] The integrated J_{sc} extracted from I−V scans that is within 20% deviation from the EQE signifies a reasonable correlation.[75]

Subsequently, we carried out EIS measurement to investigate the charge recombination characteristics of the control and F-GLU-S modified device. The EIS measurement was recorded at a bias of 0.9 V in dark condition. The EIS curve and the corresponding equivalent circuit is provided in Figure 4i, and the extracted information are summarized in Table S4. In general, the high-frequency semi-circle in the Nyquist plot ascribed the recombination resistance and geometrical capacitance.[76-77] The fitting results revealed that the series resistance of the F-GLU-S modified device reduced from 32.63Ω (control device) to 26.53Ω which leads to FF improvement. Intriguingly, the charge recombination resistance (R_2) depicted by the large semi-circle significantly enhanced above seven-fold times for the F-GLU-S passivated device compared to the control device (9545Ω Vs 1392Ω) which clearly proved the F-GLU-S significantly reduced the surface, grain boundary and electronic defects as a result the non-radiative charge recombination repressed which leads to V_{oc} improvement in the device.

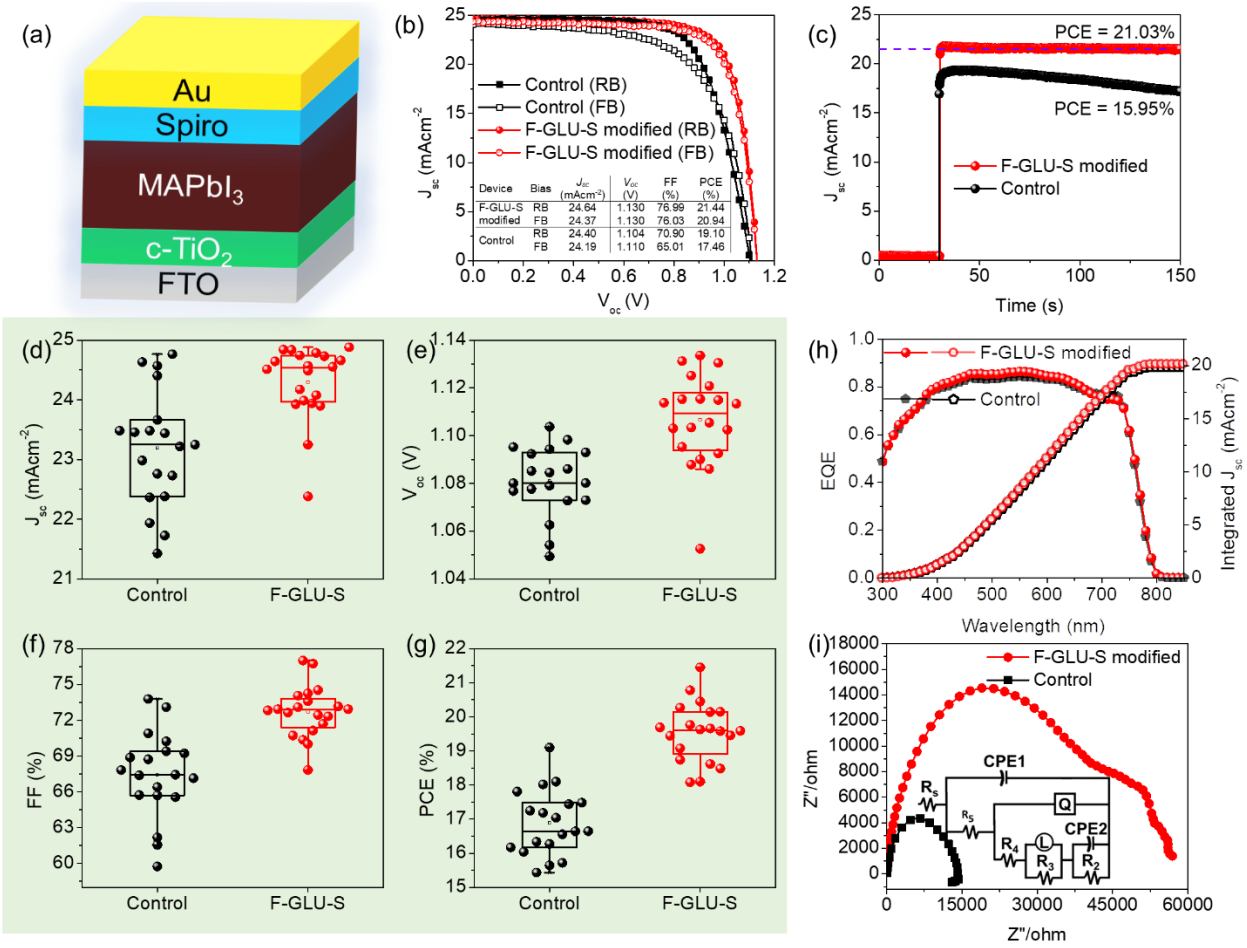

Figure 4. (a) Schematic illustration of the fabricated device with a structure of FTO/c-TiO_2/ $MAPbI_3$ with and without 2mM F-GLU-S modification/Spiro-OMeTAD/Au. (b) The champion device performance using the control and 2mM F-GLU-S modified $MAPbI_3$. (c) Stabilized power output of the control and F-GLU-S modified $MAPbI_3$ based device at maximum power point of 0.98 V. Box chart comparison of the J-V parameters for the control and 2mM F-GLU-S modified $MAPbI_3$ (d) J_{sc}, (e) V_{oc}, (f) FF and (g) PCE. (h) EQE and integrated J_{sc} of the control and 2mM F-GLU-S modified $MAPbI_3$ based device, and (i) Nyquist plots of the control and 2mM F-GLU-S modified $MAPbI_3$ based device. The inset shows their eqivalent circuit.

Finally, we studied the influence of F-GLU-S modification on the long-term device stability. In general, defects not only minimize the PCE of the PSCs but also cause device instability.[78-79] To

study the slot-die coated perovskite film stability, we measured water contact angle for both the control and F-GLU-S modified perovskite films where the control perovskite film showed a water contact angle of 53.36° (Figure 5a). Interestingly, the water contact angle increased to 72.35° (Figure 5b) for the F-GLU-S modified slot-die coated perovskite film which infers the modified film has potential to prevent the penetration of moisture better than the control perovskite film. Then, we studied the long-term stability of the control and F-GLU-S modified perovskite devices. We kept both devices in air at RH of 50-60% for one month. Four devices for each of the control and modified devices were investigated to ensure the long-term study data is reproducible. The V_{oc} of the control devices was not influenced by the moisture, implying we get highly compact TiO_2 film. However, both Jsc and FF degraded exponentially. Interestingly, the F-GLU-S modified devices exhibited impressive stability in which the devices retained ~ 92% of their initial performance after 720 h. The long-term stability of the control and F-GLU-S modified devices are shown in Figure 5c-f.

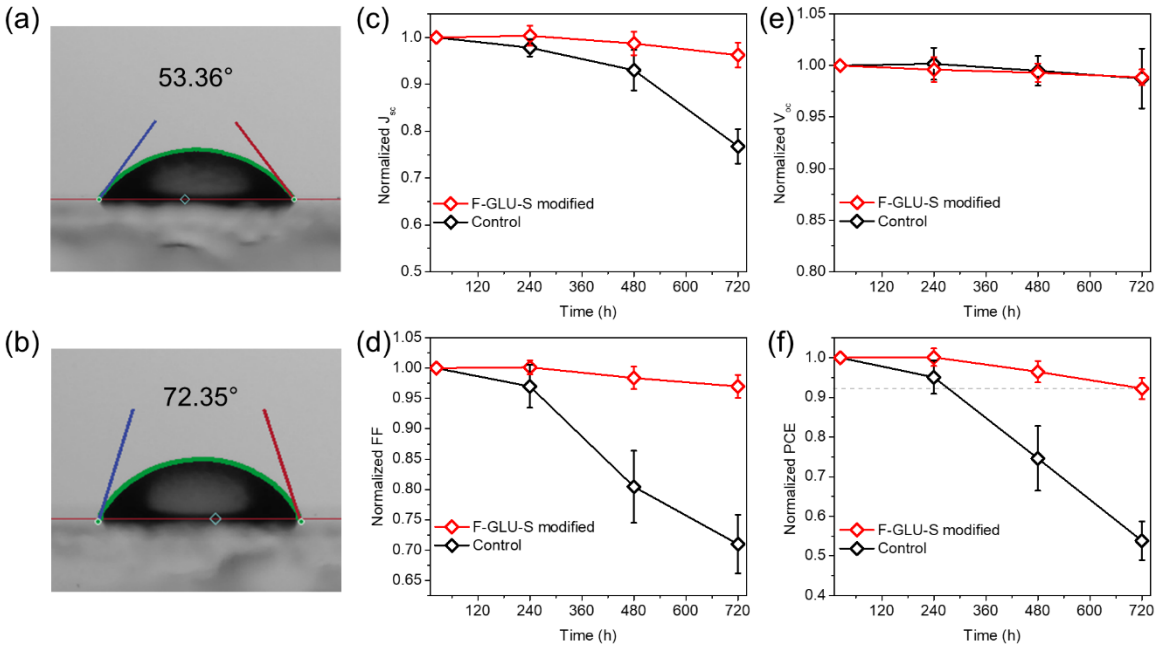

Figure 5. (a) Water contact angle of (a) the control, and (b) 2mM F-GLU-S modified $MAPbI_3$. Long-term stability of the control and 2mM F-GLU-S modified $MAPbI_3$ in air (RH= 50-60%) for 720 hours (c) J_{sc}, (d) FF, (e) V_{oc} and (f) PCE.

Conclusions

In summary, we have successfully passivated the defects of slot-die coated perovskite by a novel F-GLU-S. The FTIR characterization revealed the strong interaction between F-GLU-S and perovskite through carbonyl group (Pb-C=O) as a result the uncoordinated Pb^{2+} ions effectively suppressed which unambiguously validated with 2D-GIWAXS and XPS peak shifts. Moreover, the F-GLU-S interacted with perovskite through hydrogen bonding (N-H…Cl) thus the I^- vacancies successfully repaired. As a result, the non-radiative recombination of the modified perovskite significantly suppressed which is validated with the PL increase on the modified film. Furthermore, the modified perovskite exhibited extraordinary charge recombination resistance (seven-fold times higher) compared to the control device. The investigation on PL and EIS clearly indicated the non-radiative recombination effectively suppressed by the modification. Therefore, F-GLU-S modified slot-die coated perovskite device demonstrated excellent V_{oc} of 1.130 V and FF of 76.99% with outstanding PCE of 21.44% which is one of the highest reported results based on slot-die coated perovskite. Moreover, device fabricated from the F-GLU-S modified perovskite exhibited excellent long-term stability and retained ~92% of its initial performance after it stored a month in air at room temperature and 50-60% RT.

ASSOCIATED CONTENT

Supporting Information

Summarized table of various passivation/additive molecules used to modify the slot-die coated perovskite layer. FTIR of the control, F-GLU-S modified perovskite, and F-GLU-S powder. Zoomed Q Vector. Fitted C1s, S2p and full XPS spectra. AFM, UV-Vis, TRPL calculations, box charts and tables of photovoltaic parameters, and EIS fitting calculations.

Notes

The authors declare no competing financial interest.

Acknowledgment

This material is based on work supported by the National Science Foundation (NSF) under Grant No. 1757220. The steady-state PL and TRPL equipment used in this work is supported by National Science Foundation Research Initiation Award: Novel Perovskite Solar Cells Based on Interface Manipulation (Award#1900047). Q. Dai thanks the support of NSF-PREM grant #DMR-1826886 for the AFM measurements by N. Pradhan. XPS instrumentation used in this work was supported by the NSF Major Research Instrumentation Program (DMR-1726901). This work is also partially supported by the DOE SIPS program with award number of EE0010242.

References

1. J. Jeong, M. Kim, J. Seo, H. Lu, P. Ahlawat, A. Mishra, Y. Yang, M. A. Hope, F. T. Eickemeyer, M. Kim, Y. J. Yoon, I. W. Choi, B. P. Darwich, S. J. Choi, Y. Jo, J. H. Lee, B. Walker, S. M. Zakeeruddin, L. Emsley, U. Rothlisberger, A. Hagfeldt, D. S. Kim, M. Gratzel, J. Y. Kim,

494 Pseudo-Halide Anion Engineering for Alpha-FAPbI3 Perovskite Solar Cells, *Nature 592* (2021)
495 381-385.
496 2. H. Min, M. Kim, S.-U. Lee, H. Kim, G. Kim, K. Choi, J. H. Lee, S. I. Seok, Efficient,
497 Stable Solar Cells by Using Inherent Bandgap of a-phase Formamidinium Lead Iodide, *Science*
498 (2019) 749–753.
499 3. N. G. Park, Research Direction toward Scalable, Stable, and High Efficiency Perovskite
500 Solar Cells, *Adv. Energy Mater. 10* (2019) 1903106.
501 4. H. Higuchi, T. Negami, Largest highly efficient 203 × 203 mm2 CH3NH3PbI3 perovskite
502 solar modules, *Jpn. J. Appl. Phys. 57* (2018) 08re11.
503 5. X. Niu, N. Li, Q. Chen, H. Zhou, Insights into Large-Scale Fabrication Methods in
504 Perovskite Photovoltaics, *Adv. Energy Sustainability Res. 2* (2020) 2000046.
505 6. D.-K. Lee, N.-G. Park, Materials and Methods for High-Efficiency Perovskite Solar
506 Modules, *Sol. RRL 6* (2021) 2100455.
507 7. D. S. Ham, W. J. Choi, H. Yun, M. Kim, D.-H. Yeo, S. Lee, B. J. Kim, J. H. Lee, Influence
508 of Drying Conditions on Device Performances of Antisolvent-Assisted Roll-to-Roll Slot Die-
509 Coated Perovskite Solar Cells, *ACS Appl. Energy Mater. 4* (2021) 7611-7621.
510 8. Y. Wang, C. Duan, P. Lv, Z. Ku, J. Lu, F. Huang, Y. B. Cheng, Printing strategies for
511 scaling-up perovskite solar cells, *Natl. Sci. Rev. 8* (2021) nwab075.
512 9. H.-J. Kim, H.-S. Kim, N.-G. Park, Progress of Perovskite Solar Modules, *Adv. Energy*
513 *Sustainability Res. 2* (2021) 2000051.
514 10. E. Berger, M. Bagheri, S. Asgari, J. Zhou, M. Kokkonen, P. Talebi, J. Luo, A. F. Nogueira,
515 T. Watson, S. G. Hashmi, Recent developments in perovskite-based precursor inks for scalable
516 architectures of perovskite solar cell technology, *Sustainable Energy Fuels 6* (2022) 2879-2900.

11. J. B. Whitaker, D. H. Kim, B. W. Larson, F. Zhang, J. J. Berry, M. F. Van Hest, K. Zhu, Scalable slot-die coating of high performance perovskite solar cells, *Sustainable Energy Fuels 2* (2018) 2442-2449.

12. P. Liu, G. Tang, F. Yan, Strategies for Large-Scale Fabrication of Perovskite Films for Solar Cells, *Sol. RRL 6* (2021) 2100683.

13. E. Rezaee, D. Kutsarov, B. Li, J. Bi, S. R. P. Silva, A route towards the fabrication of large-scale and high-quality perovskite films for optoelectronic devices, *Sci. Rep. 12* (2022) 7411.

14. I. Zimmermann, M. Al Atem, O. Fournier, S. Bernard, S. Jutteau, L. Lombez, J. Rousset, Sequentially Slot-Die-Coated Perovskite for Efficient and Scalable Solar Cells, *Adv. Mater. Interfaces 8* (2021) 2100743.

15. M. Fievez, P. J. Singh Rana, T. M. Koh, M. Manceau, J. H. Lew, N. F. Jamaludin, B. Ghosh, A. Bruno, S. Cros, S. Berson, S. G. Mhaisalkar, W. L. Leong, Slot-die coated methylammonium-free perovskite solar cells with 18% efficiency, *Sol. Energy Mater. Sol. Cells 230* (2021) 111189.

16. I. Zimmermann, M. Provost, S. Mejaouri, M. Al Atem, A. Blaizot, A. Duchatelet, S. Collin, J. Rousset, Industrially Compatible Fabrication Process of Perovskite-Based Mini-Modules Coupling Sequential Slot-Die Coating and Chemical Bath Deposition, *ACS Appl. Mater. Interfaces. 14* (2022) 11636-11644.

17. M. Wang, Y. Yin, W. Cai, J. Liu, Y. Han, Y. Feng, Q. Dong, Y. Wang, J. Bian, Y. Shi, Synergetic Co-Modulation of Crystallization and Co-Passivation of Defects for FAPbI3 Perovskite Solar Cells, *Adv. Funct. Mater. 32* (2021) 2108567.

18. J. Xiong, Z. Dai, S. Zhan, X. Zhang, X. Xue, W. Liu, Z. Zhang, Y. Huang, Q. Dai, J. Zhang, Multifunctional Passivation Strategy Based on Tetraoctylammonium Bromide for Efficient Inverted Perovskite Solar Cells, *Nano Energy 84* (2021) 105882.

19. L. Tang, Yang Huang, Chen Wang, Zhenxuan Zhao, Yiming Yang, Jiming Bian, Huaqiang Wu, Zengxing Zhang, and David Wei Zhang, Halide perovskite memristor with ultra-high-speed and robust flexibility for artificial neuron applications *J. Mater. Chem. C 10* (2022) 14695-14702.

20. F. Xu, J. Liu, A. S. Subbiah, W. Liu, J. Kang, G. T. Harrison, X. Yang, F. H. Isikgor, E. Aydin, M. De Bastiani, S. De Wolf, Potassium Thiocyanate-Assisted Enhancement of Slot-Die-Coated Perovskite Films for High-Performance Solar Cells, *Small Sci. 1* (2021) 2000044.

21. M. Du, X. Zhu, L. Wang, H. Wang, J. Feng, X. Jiang, Y. Cao, Y. Sun, L. Duan, Y. Jiao, K. Wang, X. Ren, Z. Yan, S. Pang, S. F. Liu, High-Pressure Nitrogen-Extraction and Effective Passivation to Attain Highest Large-Area Perovskite Solar Module Efficiency, *Adv. Mater. 32* (2020) e2004979.

22. M. Othman, F. Zheng, A. Seeber, A. S. R. Chesman, A. D. Scully, K. P. Ghiggino, M. Gao, J. Etheridge, D. Angmo, Millimeter-Sized Clusters of Triple Cation Perovskite Enables Highly Efficient and Reproducible Roll-to-Roll Fabricated Inverted Perovskite Solar Cells, *Adv. Funct. Mater. 32* (2021) 2110700.

23. H.-J. Lee, S.-I. Na, Efficient mixed-cation perovskite photovoltaic cells via additive-assisted slot-die deposition, *Mater. Res. Bull. 149* (2022)

24. L. Tao, B. Wang, H. Wang, C. Chen, X. Ding, Y. Tian, H. Lu, X. Yang, M. Cheng, Surface Defect Passivation and Energy Level Alignment Engineering with a Fluorine-Substituted Hole Transport Material for Efficient Perovskite Solar Cells, *ACS Appl. Mater. Interfaces 13* (2021) 13470-13477.

25. P. J. S. Rana, B. Febriansyah, T. M. Koh, B. T. Muhammad, T. Salim, T. J. N. Hooper, A. Kanwat, B. Ghosh, P. Kajal, J. H. Lew, Y. C. Aw, N. Yantara, A. Bruno, S. A. Pullarkat, J. W.

562 Ager, W. L. Leong, S. G. Mhaisalkar, N. Mathews, Alkali Additives Enable Efficient Large Area
563 (>55 cm2) Slot-Die Coated Perovskite Solar Modules, *Adv. Funct. Mater. 32* (2022) 2113026.
564 26. Q. Jiang, Y. Zhao, X. Zhang, X. Yang, Y. Chen, Z. Chu, Q. Ye, X. Li, Z. Yin, J. You,
565 Surface Passivation of Perovskite Film for Efficient Solar Cells, *Nat. Photonics 13* (2019) 460-
566 466.
567 27. N. De Marco, H. Zhou, Q. Chen, P. Sun, Z. Liu, L. Meng, E. P. Yao, Y. Liu, A. Schiffer,
568 Y. Yang, Guanidinium: A Route to Enhanced Carrier Lifetime and Open-Circuit Voltage in Hybrid
569 Perovskite Solar Cells, *Nano Lett. 16* (2016) 1009-1016.
570 28. J. I. Uribe, J. Ciro, J. F. Montoya, J. Osorio, F. Jaramillo, Enhancement of Morphological
571 and Optoelectronic Properties of Perovskite Films by CH3NH3Cl Treatment for Efficient Solar
572 Minimodules, *ACS Appl. Energy Mater. 1* (2018) 1047-1052.
573 29. M. Kim, G.-H. Kim, T. K. Lee, I. W. Choi, H. W. Choi, Y. Jo, Y. J. Yoon, J. W. Kim, J.
574 Lee, D. Huh, H. Lee, S. K. Kwak, J. Y. Kim, D. S. Kim, Methylammonium Chloride Induces
575 Intermediate Phase Stabilization for Efficient Perovskite Solar Cells, *Joule 3* (2019) 2179-2192.
576 30. W. Liu, J. Xiong, N. Liu, J. Dai, Z. Dai, Y. Huang, Z. Zhang, X. Xue, Q. Dai, J. Zhang,
577 Defect Passivation and Interface Modification by Tetra-n-octadecyl Ammonium Bromide for
578 Efficient and Stable Inverted Perovskite Solar Cells, *Chem. Eng. J. 429* (2022) 132426.
579 31. Y. Shao, Z. Xiao, C. Bi, Y. Yuan, J. Huang, Origin and Elimination of Photocurrent
580 Hysteresis by Fullerene Passivation in CH3NH3PbI3 Planar Heterojunction Solar Cells, *Nat.*
581 *Commun. 5* (2014) 5784.
582 32. Y. Lin, Y. Bai, Y. Fang, Z. Chen, S. Yang, X. Zheng, S. Tang, Y. Liu, J. Zhao, J. Huang,
583 Enhanced Thermal Stability in Perovskite Solar Cells by Assembling 2D/3D Stacking Structures,
584 *J. Phys. Chem. Lett. 9* (2018) 654-658.

33. R. J. Stoddard, A. Rajagopal, R. L. Palmer, I. L. Braly, A. K. Y. Jen, H. W. Hillhouse, Enhancing Defect Tolerance and Phase Stability of High-Bandgap Perovskites via Guanidinium Alloying, *ACS Energy Lett. 3* (2018) 1261-1268.

34. E. H. Jung, N. J. Jeon, E. Y. Park, C. S. Moon, T. J. Shin, T. Y. Yang, J. H. Noh, J. Seo, Efficient, Stable and Scalable Perovskite Solar Cells using Poly(3-hexylthiophene), *Nature 567* (2019) 511-515.

35. X. Zheng, B. Chen, J. Dai, Y. Fang, Y. Bai, Y. Lin, H. Wei, Xiao C. Zeng, J. Huang, Defect Passivation in Hybrid Perovskite Solar Cells using Quaternary Ammonium Halide Anions and Cations, *Nat. Energy 2* (2017) 1-9.

36. T. Zhang, L. Xie, L. Chen, N. Guo, G. Li, Z. Tian, B. Mao, Y. Zhao, In Situ Fabrication of Highly Luminescent Bifunctional Amino Acid Crosslinked 2D/3D NH3C4H9COO(CH3NH3PbBr3)n Perovskite Films, *Adv. Funct. Mater. 27* (2017) 1603568.

37. S. Ye, H. Rao, Z. Zhao, L. Zhang, H. Bao, W. Sun, Y. Li, F. Gu, J. Wang, Z. Liu, Z. Bian, C. Huang, A Breakthrough Efficiency of 19.9% Obtained in Inverted Perovskite Solar Cells by using an Efficient Trap State Passivator Cu(thiourea)I, *J. Am. Chem. Soc. 139* (2017) 7504-7512.

38. X. Li, M. I. Dar, C. Yi, J. Luo, M. Tschumi, S. M. Zakeeruddin, M. K. Nazeeruddin, H. Han, M. Gratzel, Improved Performance and Stability of Perovskite Solar Cells by Crystal Crosslinking with Alkylphosphonic Acid Omega-Ammonium Chlorides, *Nat. Chem. 7* (2015) 703-711.

39. C. Kyoungwon, L. Junwoo, K. Hong Il, P. Cheol Woong, K. Guan-Woo, C. Hyuntae, P. Sungjin, P. Sang Ah, P. Taiho, Thermally Stable, Planar Hybrid Perovskite Solar Cells with High Efficiency, *Energy Environ. Sci.* (2018) 3238-3247.

607 40. S. Yang, J. Dai, Z. Yu, Y. Shao, Y. Zhou, X. Xiao, X. C. Zeng, J. Huang, Tailoring
608 Passivation Molecular Structures for Extremely Small Open-Circuit Voltage Loss in Perovskite
609 Solar Cells, *J. Am. Chem. Soc. 141* (2019) 5781-5787.
610 41. X. Zhou, M. Hu, C. Liu, L. Zhang, X. Zhong, X. Li, Y. Tian, C. Cheng, B. Xu, Synergistic
611 Effects of Multiple Functional Ionic Liquid-Treated PEDOT:PSS and Less-Ion-Defects S-
612 Acetylthiocholine Chloride-Passivated Perovskite Surface Enabling Stable and Hysteresis-Free
613 Inverted Perovskite Solar Cells with Conversion Efficiency Over 20%, *Nano Energy 63* (2019)
614 103866.
615 42. A. Krishna, M. A. Akhavan Kazemi, M. Sliwa, G. N. M. Reddy, L. Delevoye, O. Lafon,
616 A. Felten, M. T. Do, S. Gottis, F. Sauvage, Defect Passivation via the Incorporation of
617 Tetrapropylammonium Cation Leading to Stability Enhancement in Lead Halide Perovskite, *Adv.*
618 *Funct. Mater. 30* (2020) 1909737.
619 43. S. Y. Abate, Q. Zhang, Y. Qi, J. Nash, K. Gollinger, X. Zhu, F. Han, N. Pradhan, Q. Dai,
620 Universal Surface Passivation of Organic-Inorganic Halide Perovskite Films by
621 Tetraoctylammonium Chloride for High-Performance and Stable Perovskite Solar Cells. , *ACS*
622 *Appl. Mater. Interfaces 14* (2022) 28044-28059.
623 44. Y. Qi, K. A. Green, G. Ma, S. Jha, K. Gollinger, C. Wang, X. Gu, D. Patton, S. E. Morgan,
624 Q. Dai, Passivation of Iodine Vacancies of Perovskite Films by Reducing Iodine to Triiodide
625 Anions for High-Performance Photovoltaics, *Chem. Eng. J.* (2022) 135647.
626 45. S.-C. Yun, S. Ma, H.-C. Kwon, K. Kim, G. Jang, H. Yang, J. Moon, Amino acid salt-driven
627 planar hybrid perovskite solar cells with enhanced humidity stability, *Nano Energy 59* (2019) 481-
628 491.

46. C. T. Lin, W. Xu, T. J. Macdonald, J. Ngiam, J. H. Kim, T. Du, S. Xu, P. S. Tuladhar, H. Kang, K. Lee, J. R. Durrant, M. A. McLachlan, Correlating the Active Layer Structure and Composition with the Device Performance and Lifetime of Amino-Acid-Modified Perovskite Solar Cells, *ACS Appl. Mater. Interfaces 13* (2021) 43505-43515.

47. W. Zhang, X. Lei, J. Liu, J. Dong, X. Yan, W. Gao, H. Dong, C. Ran, Z. Wu, Efficient Charge Collection Promoted by Interface Passivation Using Amino Acid Toward High Performance Perovskite Solar Cells, *Phys. Status Solidi RRL 13* (2019) 1800505.

48. H. S. Lin, J. M. Lee, J. Han, C. Lee, S. Seo, S. Tan, H. M. Lee, E. J. Choi, M. S. Strano, Y. Yang, S. Maruyama, I. Jeon, Y. Matsuo, J. W. Oh, Denatured M13 Bacteriophage-Templated Perovskite Solar Cells Exhibiting High Efficiency, *Adv. Sci. 7* (2020) 2000782.

49. D. Jia, J. Chen, M. Yu, J. Liu, E. M. J. Johansson, A. Hagfeldt, X. Zhang, Dual Passivation of CsPbI3 Perovskite Nanocrystals with Amino Acid Ligands for Efficient Quantum Dot Solar Cells, *Small 16* (2020) e2001772.

50. J. Du, L. Feng, X. Guo, X. Huang, Z. Lin, J. Su, Z. Hu, J. Zhang, J. Chang, Y. Hao, Enhanced efficiency and stability of planar perovskite solar cells by introducing amino acid to SnO2/perovskite interface, *J. Power Sources 455* (2020) 227974.

51. J. Han, K. Kim, J. S. Nam, S. J. Hong, E. J. Choi, D. Kim, I. Chung, H. S. Lin, T. D. Kim, M. S. Strano, B. Han, J. W. Oh, H. D. Kim, I. Jeon, Genetic Manipulation of M13 Bacteriophage for Enhancing the Efficiency of Virus-Inoculated Perovskite Solar Cells with a Certified Efficiency of 22.3%, *Adv. Energy Mater. 11* (2021) 2101221.

52. B. Ma, X. Sun, S. Yan, L. Zhang, S. Chen, X. Liu, J. Song, Interface modification by Fmoc-Met-OH molecule for high-efficient perovskite solar cells, *J. Mater. Sci: Mater. Electron. 33* (2022) 15359-15368.

53. B. Hu, J. Zhang, Z. Guo, L. Lu, P. Li, M. Chen, C. Li, Manipulating Ion Migration and Interfacial Carrier Dynamics via Amino Acid Treatment in Planar Perovskite Solar Cells, *ACS Appl. Mater. Interfaces 14* (2022) 15840-15848.

54. Y. Choi, D. Koo, G. Jeong, U. Kim, H. Kim, F. Huang, H. Park, A vertically oriented two-dimensional Ruddlesden–Popper phase perovskite passivation layer for efficient and stable inverted perovskite solar cells, *Energy Environ. Sci. 15* (2022) 3369-3378.

55. S. Han, H. Zhang, Y. Li, R. Wang, Q. He, Solution-processed amino acid modified SnO2 electron transport layer for carbon-based CsPbIBr2 perovskite solar cells, *Mater. Sci. Semicond. Process. 133* (2021) 105964.

56. J. Song, Q. Qiu, X. Sun, L. Wang, Surface modification of perovskite film by an amino acid derivative for perovskite solar cell, *Org. Electron. 108* (2022) 106598.

57. P. Sang, Y. Shi, B. Huang, S. Xue, T. Odom, J. Cai, Sulfono-γ-AApeptides as Helical Mimetics: Crystal Structures and Applications, *Acc. Chem. Res. 53* (2020) 2425-2442.

58. Y. Shi, P. Sang, G. Yin, R. Gao, X. Liang, R. Brzozowski, T. Odom, P. Eswara, Y. Zheng, X. Li, J. Cai, Aggregation-Induced Emissive and Circularly Polarized Homogeneous Sulfono-gamma-AApeptide Foldamers, *Adv. Opt. Mater. 8* (2020)

59. Y. Shi, G. Yin, Z. Yan, P. Sang, M. Wang, R. Brzozowski, P. Eswara, L. Wojtas, Y. Zheng, X. Li, J. Cai, Helical Sulfono-γ-AApeptides with Aggregation-Induced Emission and Circularly Polarized Luminescence, *J. Am. Chem. Soc. 141* (2019) 12697-12706.

60. G. B. Adugna, S. Y. Abate, W. T. Wu, Y. T. Tao, Toward Large-Area and Fully Solution-Sheared Perovskite Solar Cells., *ACS Appl. Mater. Interfaces 13* (2021) 25926-25936.

673 61. D.-N. Jeong, D.-K. Lee, S. Seo, S. Y. Lim, Y. Zhang, H. Shin, H. Cheong, N.-G. Park,
674 Perovskite Cluster-Containing Solution for Scalable D-Bar Coating toward High-Throughput
675 Perovskite Solar Cells, *ACS Energy Lett. 4* (2019) 1189-1195.
676 62. S. Y. Abate, Q. Zhang, Y. Qi, J. Nash, K. Gollinger, X. Zhu, F. Han, N. Pradhan, Q. Dai,
677 Universal Surface Passivation of Organic-Inorganic Halide Perovskite Films by
678 Tetraoctylammonium Chloride for High-Performance and Stable Perovskite Solar Cells, *ACS Appl.*
679 *Mater. Interfaces 14* (2022) 28044-28059.
680 63. S. Wang, F. Cao, Y. Wu, X. Zhang, J. Zou, Z. Lan, W. Sun, J. Wu, P. Gao, Multifunctional
681 2D Perovskite Capping Layer using Cyclohexylmethylammonium Bromide for Highly Efficient
682 and Stable Perovskite Solar Cells, *Mater. Today Phys. 21* (2021) 100543.
683 64. H. Kim, M. Pei, Y. Lee, A. A. Sutanto, S. Paek, V. I. E. Queloz, A. J. Huckaba, K. T. Cho,
684 H. J. Yun, H. Yang, M. K. Nazeeruddin, Self-Crystallized Multifunctional 2D Perovskite for
685 Efficient and Stable Perovskite Solar Cells, *Adv. Funct. Mater. 30* (2020) 1910620.
686 65. J. Hu, X. Xu, Y. Chen, S. Wu, Z. Wang, Y. Wang, X. Jiang, B. Cai, T. Shi, C. J. Brabec,
687 Y. Mai, F. Guo, Overcoming photovoltage deficit via natural amino acid passivation for efficient
688 perovskite solar cells and modules, *J. Mater. Chem. A 9* (2021) 5857-5865.
689 66. C. Ma, N.-G. Park, Paradoxical Approach with a Hydrophilic Passivation Layer for
690 Moisture-Stable, 23% Efficient Perovskite Solar Cells, *ACS Energy Lett. 5* (2020) 3268-3275.
691 67. S. Y. Abate, W. T. Wu, S. Pola, Y. T. Tao, Compact TiO2 films with sandwiched Ag
692 nanoparticles as electron-collecting layer in planar type perovskite solar cells: improvement in
693 efficiency and stability, *RSC Adv. 8* (2018) 7847-7854.

68. Y. S. Lin, S. Y. Abate, K. W. Lai, C. W. Chu, Y. D. Lin, Y. T. Tao, S. S. Sun, New Helicene-Type Hole-Transporting Molecules for High-Performance and Durable Perovskite Solar Cells, *ACS Appl. Mater. Interfaces 10* (2018) 41439-41449.

69. W. Yang, R. Su, D. Luo, Q. Hu, F. Zhang, Z. Xu, Z. Wang, J. Tang, Z. Lv, X. Yang, Y. Tu, W. Zhang, H. Zhong, Q. Gong, T. P. Russell, R. Zhu, Surface modification induced by perovskite quantum dots for triple-cation perovskite solar cells, *Nano Energy 67* (2020)

70. S. Y. Abate, D.-C. Huang, Y.-T. Tao, Surface modification of TiO2 layer with phosphonic acid monolayer in perovskite solar cells: Effect of chain length and terminal functional group, *Org. Electron. 78* (2020)

71. Q. Chen, K. Deng, Y. Shen, L. Li, Stable One Dimensional (1D)/Three Dimensional (3D) Perovskite Solar Cell with an Efficiency Exceeding 23%, *InfoMat. 4* (2022) e12303.

72. E. A. Alharbi, A. Y. Alyamani, D. J. Kubicki, A. R. Uhl, B. J. Walder, A. Q. Alanazi, J. Luo, A. Burgos-Caminal, A. Albadri, H. Albrithen, M. H. Alotaibi, J. E. Moser, S. M. Zakeeruddin, F. Giordano, L. Emsley, M. Gratzel, Atomic-Level Passivation Mechanism of Ammonium Salts Enabling Highly Efficient Perovskite Solar Cells, *Nat. Commun. 10* (2019) 3008.

73. H.-S. Kim, J.-Y. Seo, S. Akin, E. Simon, M. Fleischer, S. M. Zakeeruddin, M. Grätzel, A. Hagfeldt, Power output stabilizing feature in perovskite solar cells at operating condition: Selective contact-dependent charge recombination dynamics, *Nano Energy 61* (2019) 126-131.

74. J. Kim, J. S. Yun, Y. Cho, D. S. Lee, B. Wilkinson, A. M. Soufiani, X. Deng, J. Zheng, A. Shi, S. Lim, S. Chen, Z. Hameiri, M. Zhang, C. F. J. Lau, S. Huang, M. A. Green, A. W. Y. Ho-Baillie, Overcoming the Challenges of Large-Area High-Efficiency Perovskite Solar Cells, *ACS Energy Lett. 2* (2017) 1978-1984.

75. J. A. Christians, J. S. Manser, P. V. Kamat, Best Practices in Perovskite Solar Cell Efficiency Measurements. Avoiding the Error of Making Bad Cells Look Good, *J. Phys. Chem. Lett. 6* (2015) 852-857.

76. A. Bou, A. Pockett, D. Raptis, T. Watson, M. J. Carnie, J. Bisquert, Beyond Impedance Spectroscopy of Perovskite Solar Cells: Insights from the Spectral Correlation of the Electrooptical Frequency Techniques, *J. Phys. Chem. Lett. 11* (2020) 8654-8659.

77. A. Guerrero, J. Bisquert, G. Garcia-Belmonte, Impedance Spectroscopy of Metal Halide Perovskite Solar Cells from the Perspective of Equivalent Circuits, *Chem. Rev. 121* (2021) 14430-14484.

78. D.-H. Kang, S.-Y. Kim, J.-W. Lee, N.-G. Park, Efficient Surface Passivation of Perovskite Films by a Post-Treatment Method with a Minimal Dose, *J. Mater. Chem. A 9* (2021) 3441-3450.

79. M. M. Byranvand, M. Saliba, Defect Passivation of Perovskite Films for Highly Efficient and Stable Solar Cells, *Sol. RRL 5* (2021) 2100295

TOC

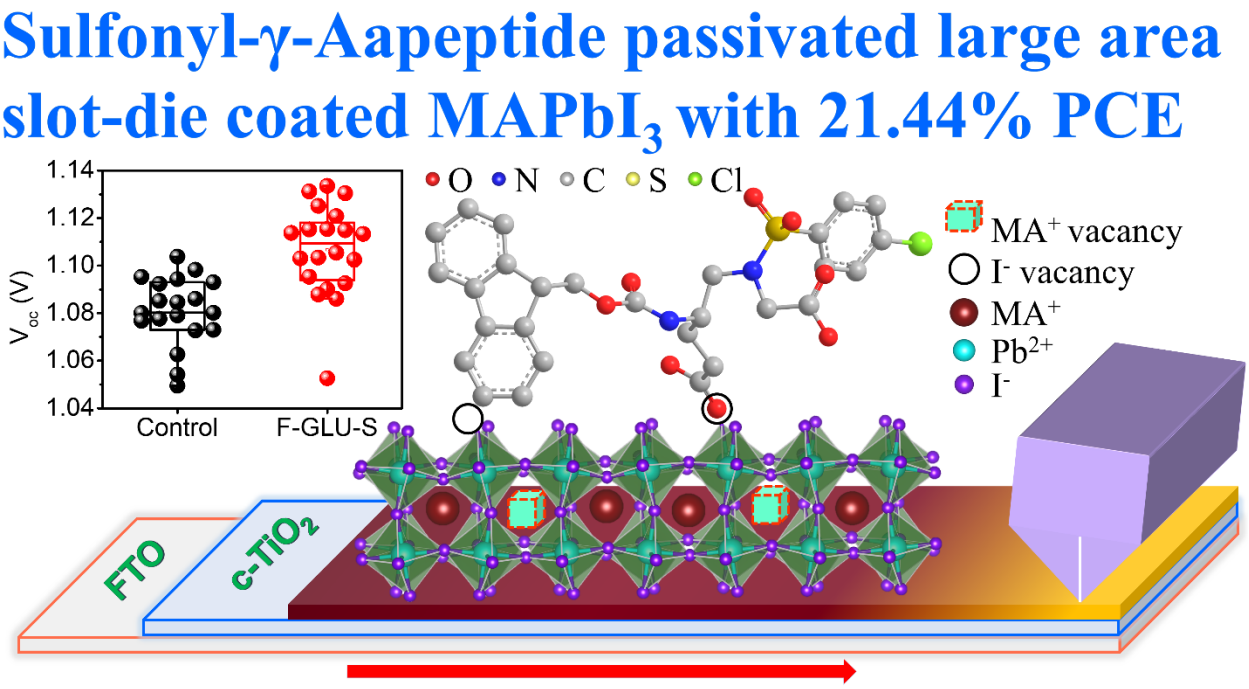

Highlights

- Large area perovskite layer slot-die coated on CBD prepared c-TiO_2 at room temperature
- The multi-functional F-GLU-S strongly coordinated with perovskite through Pb-C=O/N/O and N-H…Cl and modify the uncoordinated Pb^{2+} ions and I^- vacancy concurrently

- F-GLU-S treatment improved PL, V_{oc} and charge recombination resistance significantly
- F-GLU-S modified slot-die coated planar perovskite device produced 21.44% PCE